High-Modulus Polyethylene Fiber Structure As Shown by X-ray Diffraction

David T. Grubb* and Keshav Prasad†

Department of Materials Science and Engineering, Cornell University, Ithaca, New York 14853

Received February 20, 1992; Revised Manuscript Received April 30, 1992

ABSTRACT: High-quality X-ray diffraction patterns were obtained from small bundles and single fibers of polyethylene at both small and wide angles using a synchrotron X-ray source. The equatorial streak in small angle (SAXS) can be used to give the length, width, and misorientation of the scattering objects, while the shape of wide-angle spots gives the same information about the crystals. The SAXS objects are 150–200 nm long, longer than the crystal length. This is in accord with microfibril models where the crystals are not continuous. The fibril interfaces are significantly less well oriented than the crystals within them. This seems anomalous, but the misorientation could correspond to tapered or irregular fibrils. The crystals are 15–30 nm across, but in some samples the fibrils are apparently only 6 nm across on average. The widths could really be the same if the fibril size distribution is broad or if fibril volume fraction has been underestimated. The method of analyzing the SAXS equatorial streak can be applied to any reasonably well oriented fiber that has a fibrillar structure.

Introduction

Small-angle X-ray scattering (SAXS) is a standard method for investigating the structure of oriented polymers.[1-3] The scattering is produced by inhomogeneity of the sample, from objects usually on the 5–100-nm scale. the scattering intensity is proportional to the square of the density difference between two adjacent regions. In crystalline polymer fibers there may be three phases; these are the crystalline and amorphous regions of the polymer and microvoids. Their densities in polyethylene (PE) are approximately 1.0, 0.85, and 0 g cm^{-3}, so the scattering due to a given volume fraction of voids is 50 times stronger than from the same fraction of amorphous regions.

In many cases the polymer contains regularly packed crystalline lamellae and amorphous interlamellar regions on the scale of 10 nm. This gives a maximum in the scattering intensity, which is not related to voids and allows the lamellar "long period" and orientation to be determined and compared to the crystal orientation derived from wide-angle scattering.[4-7] The high-modulus fibers studied here have no regular lamellar structure, and the small-angle pattern is an equatorial streak of continuously diminishing intensity.[8-10] A streak similar to this is seen in many natural and synthetic fibers,[1,3,11-17] and it is often described as "void scattering". In many cases there are void fractions in fibers that may be detected by other means, and the scattering is also seen in amorphous fibers. In these cases the shape and intensity of the void scattering relate to the size, orientation, and volume fraction of voids.

In other cases the scattering may be due to both voids and the crystal morphology. A SAXS study of PE fibers at different stages of preparation from the gel has been made which explicitly considers the three-phase structure in analyzing SAXS.[10,17] It concluded that there were large void fractions in the solvent-extracted gel fibers, but the high-modulus hot-drawn fibers had few voids. The void fraction was estimated to be 1% from measurement of absolute scattering intensities. This would mean that one-third of the scattering was due to the voids.

In a study of Kevlar fibers, the SAXS scattering was taken to be entirely due to voids.[15] The scattering was much reduced when the fiber adsorbed water, and chemical treatment with H_2S and $AgNO_3$ deposited silver inside the fibers. Filling voids with any liquid will dramatically reduce the scattering they produce, and silver sulfide infiltration is a standard method in textile science for outlining internal voids in fibers. Such methods are not always reliable, as internal voids may not be accessible to liquids and the amorphous phase may absorb the liquid, changing its density and scattering. In another study, the same scattering from Kevlar was assigned to the crystalline structure.[9] The basis for this assignment was comparison with wide-angle X-ray scattering (WAXS). The size and shape of WAXS spots can be analyzed to give the length, width, and orientation of the crystalline diffracting objects. It was found that these parameters were very close to the same parameters derived from SAXS. Thus if the SAXS is derived from voids, they would have to be the same size and shape as the crystals. The simpler model was that the SAXS pattern came from the crystals themselves.

This study describes SAXS data and its comparison with WAXS for high-modulus PE fibers. There is no direct evidence for three phases, which would require absolute intensity measurements in X-ray diffraction or other techniques such as NMR.[18] Interpretation is therefore given in terms of two phases. These are taken to be the crystals and interfibrillar disordered material rather than PE and void, for reasons which will be described in the discussion section. On this interpretation, the objects giving the small-angle scattering are fibrils rather than voids. To avoid the clumsy circumlocution of "small-angle scattering object" they are called fibrils throughout the text. For interpreting SAXS streaks from fibers in terms of two phases, a series of papers by Perret and Ruland[12-14,19] on carbon fibers are an important source, including detailed discussion of some of the problems that may arise, such as multiple scattering and reflection.[10,13]

Good estimates of the orientation distribution of crystals and fibrils can be made because small fiber bundles and single fibers were the specimens. The intense focused beam of X-rays allows small instrumental beam sizes which permit useful extrapolation to the (000) beam size and thus the sizes of the scattering objects.

† Present address: IBM General Technology Division, Hopewell Junction, NY 12533.

0024-9297/92/2225-4575$03.00/0

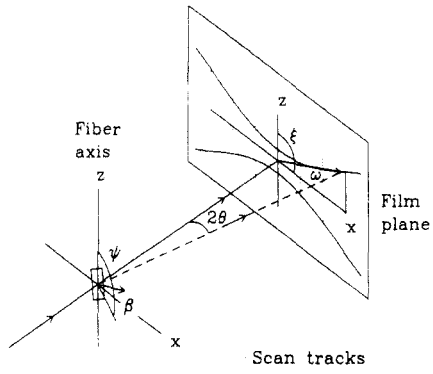

Figure 1. Schematic diagram of diffraction from a fiber sample. The normal to the diffracting object is shown at an angle ψ to the fiber axis and $\beta = 90 - \psi$ to the equator. The diffracted intensity appears at ξ to the z axis; $\omega = 90 - \xi$ on the film plane. The dotted line show the tracks of the microdensitometer when measuring the axial extent of the SAXS equatorial streak.

Experimental Section

The X-ray source was the A-1 beam line at CHESS (Cornell High Energy Synchrotron Source). This has a double-focusing monochromator, giving an intense beam of X-rays of wavelength 0.155 nm (8 keV). There is a flux of 5×10^{11} photons/s in the 0.3×1 mm focused spot. A curved crystal and curved mirror produce the focal point at the center of the experimental work space, near the detector plane. The mirrors are some distance from the focal point so the divergence is small. There is a vertical divergence of about 1 mrad and a horizontal convergence of about 2 mrad. In these experiments a pinhole collimator 200 or 500 μm in diameter was placed just before the specimen. This defines the area illuminated, and the beam diameter will be very close to the pinhole size.

The materials used were commercial Spectra 900 and Spectra 1000 (Allied Signal) and a 1-mm-wide tape kindly supplied by Prof. R. S. Porter. This tape was produced by extruding a single-crystal mat in the solid state by 6× and then drawing the product 50× at 125 °C for a total extension ratio of 300. Its modulus, crystallinity, and strength are extremely high.[16] The commercial fibers are 28 and 38 μm in diameter, so for most of the work small bundles about 300 μm across were used as samples. Some wide-angle diffraction was performed on single 28-μm-diameter filaments of Spectra 1000. Film was used to record the diffraction patterns. For SAXS the camera length was 760 mm, and for WAXS it was 40 or 65 mm. Only the equatorial reflections were recorded. Exposure times for WAXS were a few minutes and 25 min for SAXS.

A Joyce-Loebl microdensitometer was used to collect data from the films; the scan aperture was 50×500 μm. In WAXS, scans were made from the center out along the equator and perpendicular to the equator through each reflection. For SAXS, the only feature is a continuous streak in the equatorial direction. Scans were made from the center out along the equator, the x axis in Figure 1, and parallel to the z axis, one scan every millimeter as shown in Figure 1. The optical densities were in the range where density is proportional to intensity.

Data Analysis

In a previous study the full width at half-maximum (fwhm) was used to describe the width,[9] but here we use integral breadth (IB) as a more precise though less accurate measure of width. The reduced accuracy arises because the integral breadth is more sensitive than the fwhm to the choice of background subtracted from the data peak. Using integral breadth for peak width in the determination of crystal size has a special advantage when the crystals have a distribution of sizes. The size determined using IB is the volume average of the distribution; that is, the dimension perpendicular to the reflecting planes is weighted by the volume of the crystal in the average.[20] The fwhm was also determined, not for use as a direct measure of peak width but to obtain the ratio IB/fwhm. This was used as an indication of the shape of the intensity distribution. For a Gaussian distribution, this number is $(\pi/4 \ln 2)^{1/2} = 1.06$, while for a Cauchy distribution it is 1.5.

The addition of two or more sources of broadening is complex unless both distributions have the same simple form. If two sources are both Cauchy and have integral breadths a and b, then the total IB will be $(a + b)$. If both are Gaussian, then the total IB will be $(a^2 + b^2)^{1/2}$. Generally, the distributions found lie between these two extreme forms. A useful approximation for the convolution of a Cauchy distribution with a Gaussian is that the total integral breadth is $a/2 + [(a/2)^2 + b^2]^{1/2}$. Here a is the IB of the Cauchy distribution and b is the IB of the Gaussian distribution.[20]

In these experiments the background was removed by fitting a second-order polynomial to the background and subtracting it. The range of data excluded from the fit, which is an upper limit to the extent of the peak, was a human choice subject to systematic errors. The peak height was determined by fitting a parabola to the top 15% of the peak (30% for weak and noisy peaks), and this divided by the peak area gives the integral breadth. The fwhm was determined by fitting a sum function of a Gaussian and a Cauchy to the data (after background subtraction) and taking the fwhm of the fitted function.

The measurement of crystal orientation from flat-film X-ray diffraction patterns is a standard problem in texture analysis.[20] Let ψ be the angle between the fiber axis and the normal to the (hkl) reflecting plane (this is usually called ϕ, but ϕ will be used later as a volume fraction). Let ξ be the angle between the fiber axis direction and the line drawn on the film from the (000) to the (hkl) spot. Then the relation between ψ and ξ is $\cos \psi = \cos \theta \cos \xi$, where θ is the Bragg angle. As the ($hk0$) planes used in this work are almost 90° from the fiber axis, it is more convenient here to replace the misorientation angles referred to the fiber axis with the misorientation from the equator, $\beta = 90° - \psi$, and $\omega = 90° - \xi$ (see Figure 1). Then we have

$$\sin \beta = \cos \theta \sin \omega \tag{1}$$

If misorientation causes the displacement on the film of the reflection from the exact equator to be z and C is the camera length, then

$$\sin \omega = z/(C \tan 2\theta) \tag{2}$$

$$z = \frac{C \sin \beta \tan 2\theta}{\cos \theta} = \frac{2C \sin \beta \sin \theta}{\cos 2\theta} \tag{3}$$

Since we are interested in the range of orientation of crystals about the mean, z is replaced by Δz, the width of the reflection, and β will be the width of the orientation distribution. If the material has fiber symmetry so that all ($hk0$) planes are equally misoriented, then the results from all ($hk0$) reflections can be combined using the same value of β.

Misorientation of the crystals from exact alignment of the c axis along the fiber axis will cause the wide-angle reflections to spread in a circumferential manner. This spread will be convoluted with the angular width due to the finite crystal size and with instrumental broadening. Generally, the combination of all these effects will be very complicated, but here the misorientation is small, usually less than 10°, so the circumferential spread is well approximated as a linear spread perpendicular to the line drawn on the film from the (000) to the (hkl) spot. Thus the broadening of equatorial reflections due to misorientation will be added to the effect of axial crystal size L. The crystal size broadening of the equatorial peaks in the

axial direction is λ/L (assuming a Scherrer factor of unity) so that $\Delta z = \lambda C/(L \cos 2\theta)$ for a flat film. Neglecting instrumental beam size for the present, if all the distributions are Cauchy, then

$$\frac{\Delta z \cos 2\theta}{\lambda C} = 1/L + \sin \beta s \tag{4}$$

where $s = 2 \sin \theta/\lambda$. If, on the other hand, we use the common assumption that the size broadening is Cauchy and the distribution of orientation is Gaussian, then

$$\frac{\Delta z \cos 2\theta}{\lambda C} = \frac{1}{2L} + \left[\frac{1}{4L^2} + \sin^2 \beta s^2\right]^{1/2} \tag{5}$$

In either case, the integral breadth of the angular distribution β and the crystal length L can be estimated from the variation of Δz with s.

An exactly similar analysis can be performed on the equatorial streak appearing in SAXS from the same fibers. As the angles are all small, the equations above could be simplified, but in the following the full formulas have been retained. When the distance from the origin is small, a linear scan in the axial direction and a circumferential scan become more different. with the data and minimum distance from the origin used here, the error in breadth due to this problem in SAXS was found to be only 1–2%.

In both WAXS and SAXS one result of this analysis is the integral breadth β of an angular distribution. In WAXS it is the distribution of ($hk0$) planes, and the sample has been assumed to have fiber symmetry, so all such planes have the same misorientation. Since any two perpendicular ($hk0$) planes will both be misoriented by β, the misorientation of the molecular chain direction, [001], must be $\alpha = 2^{1/2}\beta$. Similarly, the SAXS result refers to the orientation of interfaces which are close to parallel to the fiber axis. If the fibrils are prismatic in shape, so that the interface normals are perpendicular to the major axis, then the misorientation of that axis from the fiber axis will again be $\alpha = 2^{1/2}\beta$.

It is not usual to express the misorientation in terms of an integral breadth of the angular distribution. Normally, the root mean square (rms) value of α, $\overline{\cos^2 \alpha}$, or the orientation function $(3\overline{\cos^2 \alpha} - 1)/2$ is used. These are all expressions of the variance. If the orientation distribution is Gaussian, and it is often assumed to be of this form, then the rms value of α will be (IB of α)/$(2\pi)^{1/2}$ or (IB of β)/$\pi^{1/2} = 0.56\beta$. In the range $0 < \beta < 10°$, the square of the cosine of this angle will also be a good estimate of $\overline{\cos^2 \alpha}$. In the same range of small β, the $\overline{\cos^2 \alpha}$ of a Cauchy distribution is essentially constant and entirely controlled by its long tails. Some peak shapes at larger values of s, where orientation dominates peak width (eq 5) were taken as an estimate of the shape of the orientation distribution. The rms values of β were found to be 0.35 IB, close to the Gaussian value.

The width of the equatorial WAXS spots in the equatorial direction can be used to derive a lateral width W and a distortion parameter for the crystals. The data do not contain several orders of the same reflection, so all the ($hk0$) spots were treated as if they were orders of the same reflection. This treatment is equivalent to assuming that the crystals are cylindrical or have a random cross section, with no ($hk0$) lattice planes longer than others. As this is not likely to be true, the more complex Fourier transform analysis of line profile was not used. Instead the angular integral breadth due to crystal distortion was taken to be $\Delta(2\theta) = 4\epsilon \tan \theta$, where $\epsilon \approx \Delta d/d$, a measure of lattice distortions.[20] The integral breadth due to finite crystal size is $\Delta(2\theta) = \lambda/W \cos \theta$, and for flat-film geometry the lateral width is $\Delta x = \Delta(2\theta)C/\cos^2 2\theta$. Neglecting the instrumental beam width at the present, for Cauchy distributions

$$\Delta x = \frac{C}{\cos^2 2\theta}\left(\frac{\lambda}{W \cos \theta} + \frac{4\epsilon \sin \theta}{\cos \theta}\right) \tag{6}$$

$$\frac{\Delta x \cos^2 2\theta \cos \theta}{\lambda C} = \frac{1}{W} + 2\epsilon s \tag{7}$$

If we assume that the size broadening is Cauchy and the distribution of orientation is Gaussian

$$\frac{\Delta x \cos^2 2\theta \cos \theta}{\lambda C} = \frac{1}{2W} + \left[\frac{1}{4W^2} + (2\epsilon s)^2\right]^{1/2} \tag{8}$$

When there is a small-angle reflection on the meridian, its width can be used to determine the lateral size of the scattering objects.[21] Here there is only the streak in SAXS. Its intensity profile in the equatorial direction is analyzed using Porod's law to give the density of interfacial surface parallel to the fiber axis. Porod's law describes the scattered intensity I at the large-angle limit (of SAXS). The structure causing the scattering must have two phases with a sharp interface between them. If S/V is the interface area per unit volume and ρ_1 and ρ_2 are the densities of the two phases, then the intensity is given by

$$\lim_{s \to \infty} I = \frac{(\rho_1 - \rho_2)^2 S}{8\pi^3 s^4 V}$$

If the densities are not known, they can be replaced by the scattering invariant Q and the volume fraction of one phase, ϕ.[3,22]

$$Q = 4\pi \int_0^\infty s^2 I(s)\, ds = \phi(1 - \phi)(\rho_1 - \rho_2)^2$$

In this limit, $Is^4 = K + As^4$, where A is a constant allowing for error in the chosen background level, so a plot of Is^4 versus s^4 should be a straight line with an intercept of K at $s = 0$. Here a plot of Is^4/Q versus s^4 is used to permit comparison between samples. This has an intercept of K/Q at $s = 0$. To determine Q, the scattered intensity was extrapolated as a straight line to zero s and a correction term of K (upper limit of integration for Q) was added to allow for scattering to higher angles. The scattering objects were assumed to be cylindrical rods, mean diameter $\bar{D}$, with a volume fraction of ϕ. Then for a unit length of material containing one rod, $S = \pi D$, $V = \pi D^2/4\phi$, and $S/V = 4\phi/D$, so

$$\bar{D} = \frac{1}{2\pi^3(1 - \phi)}\left(\frac{Q}{K} + \frac{1}{s_{max}}\right) \tag{9}$$

The volume fraction of the rodlike fibrils ϕ is not known, but if the interfibrillar material is disordered and the fibrils are not fully crystalline, then $V_c \le \phi \le 1$, where V_c is the volume fraction of crystallinity. Taking the crystallinity to be 0.8 for the gel-drawn fibers and >0.9 for the drawn tape,[16] we assume here that ϕ is 0.9 for the Spectra fibers and 0.95 for the drawn tape. Since the width derived from Porod analysis depends on $1/(1 - \phi)$, these choices will have a large effect on the results for fibril width. Qualitatively this is because the fibrils are much wider than the interfibrillar regions, and it is the distance between two interfaces across the interfibrillar gap that controls the SAXS scattering pattern. The nearer the fibrils are to volume filling, the larger they must be to maintain the size of these interfibrillar regions.

Results

Measurement of instrumental beam width was not entirely satisfactory. Direct exposures to the main beam

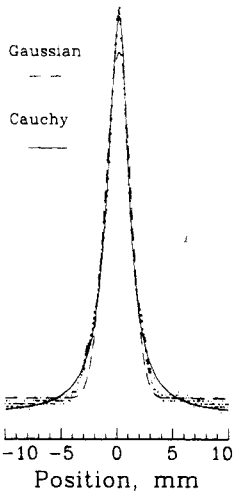

Figure 2. Typical intensity profile of an (*hk*0) reflection taken in the c axis direction. The data points are dots, reduced in size in the tails to the peak for clarity. The solid line is the best fit using a Cauchy distribution, and the dashed line is the best fit using a Gaussian distribution. The Cauchy fit overestimates the tails, and the Gaussian fit underestimates the peak.

all turned out to be overexposed, so that the peak shape could not be determined. It could be seen that the beams were sharply cut off, with very low intensities in any extended tails. Since the additive integral breadths of Cauchy distributions are due to their long tails, any sharply cut off profile is better approximated by a Gaussian. Therefore the experimental IB were corrected to $(\Delta^2 - B^2)^{1/2}$ in all cases, even when the resulting distribution was assumed Cauchy. The inconsistency in this treatment could be removed at the cost of some numerical complexity; for example

$$\frac{\Delta z \cos^2\theta}{\lambda C} = \frac{1}{2L} + \left[\frac{1}{4L^2} + \left(\frac{B}{\lambda C}\right)^2 + \sin 2\beta s^2\right]^{1/2} \quad (10)$$

is more consistent with a Cauchy distribution from size broadening, and Gaussian distributions from the instrumental beam width and from misorientation. Trials were made using this expression to fit the data and with eq 5 modified to account for the instrumental beam width. The difference in the results for L, β, W, and ϵ were much less than the uncertainty in those results. For bundle and tape samples the apparent size of the overexposed main beam was used as the integral breadth, which is an upper estimate. When single fibers are used, the effective beam size and shape are controlled by the part of the beam that the sample intercepts, which may vary from exposure to exposure. This means that for single fibers the equatorial beam size B_2 is extremely small, and the axial beam size B_1 depends on the length of the fiber that intercepts the beam.

The raw data for the crystal length and misorientation are the intensity profiles of equatorial WAXS spots, measured in the axial or meridional direction. Figure 2 shows one such profile, and superimposed upon it the best fits that can be obtained using a Cauchy, a Gaussian, and the fitting function used in determining the fwhm. The profile is clearly neither Cauchy nor Gaussian and has an integral breadth of 1.3 times the fwhm. Similar shapes can be created by convoluting a Cauchy with a Gaussian. The instrumental beam width, B_1, was very close to the collimator diameter, 0.2 mm. This was subtracted from the IB as described above, and the result was multiplied by $\cos 2\theta/(\lambda C)$ to plot as a straight line using eq 4.

The data for the tape and fiber bundles are shown in Figure 3. In this plot the intercept at $s = 0$ is 1/(axial length of the crystals). The best straight line fit through

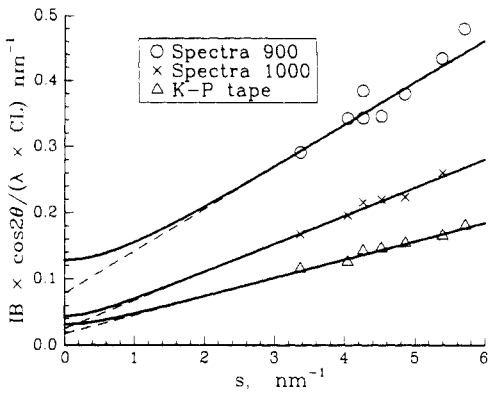

Figure 3. Axial integral breadths of equatorial (*hk*0) reflections plotted as a function of the scattering vector s. The integral breadths are geometrically corrected and normalized so that the intercept at $s = 0$ is $1/L$. The straight dashed lines correspond to an assumption of all Cauchy line profiles, and the solid lines to a Cauchy profile for crystal size and a Gaussian profile for orientation distribution.

Table I
Axial Crystal Length and Crystal Misorientation in PE Fibers

material	fitting	best L, nm	range of L, nm	β, deg
Spectra 900	C–C	12.7	7–25	3.6 ± 0.6
	C–G	7.8	5–13	3.7 ± 0.5
	G–G	6.0	4.5–8	4.1 ± 0.4
Spectra 1000	C–C	38	25–85	2.4 ± 0.2
	C–G	21	15–43	2.5 ± 0.2
	G–G	13	11–20	2.6 ± 0.1
K-P drawn tape	C–C	57	30–130	1.6 ± 0.2
	C–G	32	18–60	1.6 ± 0.15
	G–G	20	14–27	1.7 ± 0.1
Spectra 1000 single fiber	C–C	63	36–∞	1.5 ± 0.3
	C–G	37	22–1200	1.5 ± 0.3
	G–G	25	18–65	1.6 ± 0.2

each set of data is shown as a dashed line, which corresponds to the assumption of Cauchy distributions for size and misorientation elements of the line broadening (eq 4). In the fit, the points were weighted by the peak heights of the reflection. This allows for the low accuracy of the IB of weak reflections. The solid lines in the figure are obtained on the assumption that the size broadening is Cauchy and the distribution of misorientation is Gaussian. The data are fitted using eq 5, weighting the data by IB as before. It is normal to assume these forms for the distributions. In this case there is other evidence to support it; for example, the (002) intensity profile of a single Spectra 1000 fiber, which is broadened by the same size effect, is very close to a Cauchy. When orientation dominates the peak shape, at high s in Figure 3, the peak shape is close to Gaussian.

It can be seen at once from the figure that the data do fall on three straight lines. The results for both fitting methods are shown in Table I, which also includes the result of assuming all distributions to be Gaussian. Clearly, the slope is well defined and does not depend strongly on the fitting procedure used. The intercept is poorly defined and does depend strongly on the fitting method. The measurement of these equatorial spots is a good way to measure crystal alignment and a poorer way to measure crystal length. The results for axial length L are expressed as a range, rather than a standard deviation about a mean, because L is the reciprocal of the intercept.

The angular distribution of the crystals is useful for comparison with the small-angle X-ray results from the same samples. However, it may be dominated by the alignment of fibers in the bundle when the crystals in a single fiber are very well oriented. Figure 4 allows a

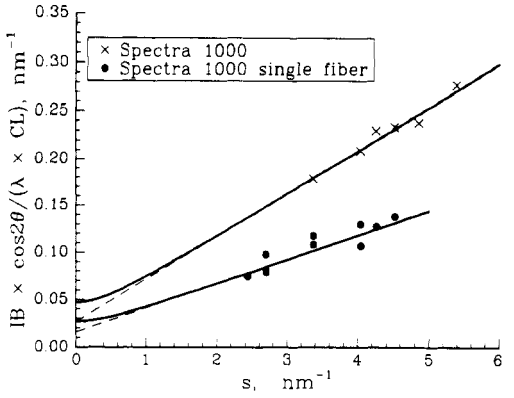

Figure 4. Axial integral breadths of equatorial (*hk*0) reflections plotted as a function of the scattering vector *s* as in Figure 3. This plot compares the data from a fiber bundle and from a single fiber of the same material. The single fiber should give a smaller slope and the same intercept.

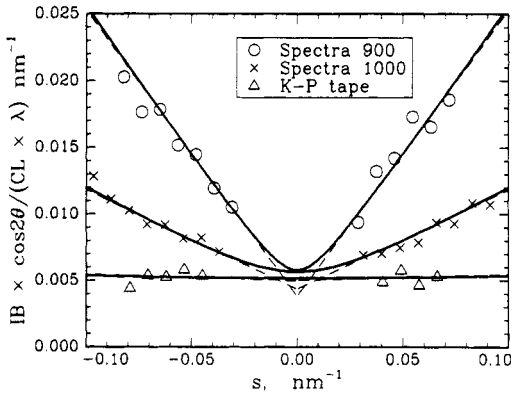

Figure 5. Axial integral breadths of the equatorial small-angle scattering streak plotted as a function of the scattering vector *s*. The integral breadths are geometrically corrected and normalized so that the intercept at $s = 0$ is $1/L$. The straight dashed lines correspond to an assumption of all Cauchy line profiles, and the solid lines to a Cauchy profile for crystal size and a Gaussian profile for orientation distribution.

Table II
Axial Fibril Length and Interface Misorientation in High-Modulus PE Samples

material	fitting	best L, nm	range of L, nm	β, deg
Spectra 900	C–C	261	220–330	12.4 ± 1.0
	C–G	172	150–205	13.0 ± 0.9
	G–G	145	130–165	14.7 ± 0.8
Spectra 1000	C–C	230	210–250	4.2 ± 0.5
	C–G	176	167–187	5.0 ± 0.4
	G–G	169	162–176	6.2 ± 0.3
K-P drawn tape	C–C	200	170–240	0.2 ± 0.9
	C–G	193	180–210	0.6 ± 2
	G–G	193	180–210	0.8 ± 3

comparison of the axial width of (*hk*0) spots from Spectra 1000 in the form of a bundle and as a single fiber. For the single fiber the collimator diameter was 0.5 mm, and the lower intensity recorded has given data at lower *s*. The results for the single fiber are given in Table I.

The axial length and misorientation of the fibrils can be determined by measuring the axial width of the equatorial streak in SAXS. Figure 5 shows the results for the same fiber bundles that were used for the WAXS analysis above. The same fitting procedures were used to give straight dashed lines and solid curves that correspond to all Cauchy and to Cauchy plus Gaussian, respectively. The results are given in Table II, which as for the WAXS case, includes the results of assuming all distributions are Gaussian. Since the data are obtained at much smaller values of *s* than in WAXS, the intercept is much less affected by the fitting procedure. The intercepts are much smaller, near 0.005 nm^{-1}.

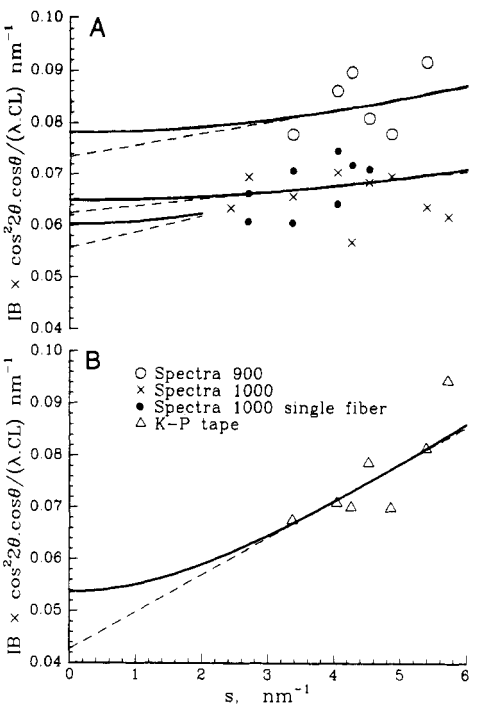

Figure 6. Equatorial integral breadths of equatorial (*hk*0) reflections plotted as a function of the scattering vector *s*. The integral breadths are geometrically corrected and normalized so that the intercept at $s = 0$ is $1/W$. The straight dashed lines correspond to an assumption of all Cauchy line profiles, and the solid lines to a Cauchy profile for crystal size and a Gaussian profile for crystal distortion. The truncated lines correspond to the data for the single fiber of Spectra 1000. The data for the drawn and extruded tape are shown separately in the lower plot because they overlap the other data.

Lateral width of crystals in the fibers is determined from measurement of integral breadths of WAXS (*hk*0) reflections in the equatorial direction. Again the instrumental beam width B_2 was found to be near the collimator diameter of 0.2 mm. This was subtracted as discussed above, and the corrected data were multiplied by $\cos^2 2\theta \cos\theta/(\lambda C)$ to plot as a straight line using eq 7. Figure 6A shows the data for bundles of Spectra fibers and for the single fiber of Spectra 1000. In the single-fiber case the effective beam size B_2 for equatorial widths is the diameter of the sample, which is negligible, so the experimental integral breadth does not need to be corrected before use. Data in the same format for the extruded and drawn tape are shown in Figure 6B.

The best straight line fit through each data set, which corresponds to the assumption that all the distributions are of Cauchy form, is again shown as a dashed line in the figures. As in the axial case, the points were weighted by the peak heights of the reflection in the fit to allow for the low accuracy of the IB of weak reflections. The accuracy of the IB was in general less than that for the axial measurements above, because of the uneven baseline due to an amorphous fraction and because the tails of the peaks could interfere with each other. As in the axial case, again, the solid curves are the best fits on the assumption that the size broadening gives a Cauchy profile and the width that increases with diffraction angle, due to distortion in this case, is Gaussian. The solid lines are the nonlinear least squares best fit to eq 8, with the same weighting by peak heights.

The extrapolation to $s = 0$ in Figure 6 is a long one, but the effect of lattice distortion, the slope of the curves, is quite small. A reasonable value for crystal width can then be obtained. The reflection widths of the extruded tape

Table III
Lateral Crystal Width and Distortion in High-Modulus PE Samples

material	fitting	best W, nm	range of W, nm	ϵ, %
Spectra 900	C–C	13.6	11–17	0.1 ± 0.2
	C–G	12.8	11–15	0.2 ± 0.2
	G–G	12.7	11–14	0.3 ± 0.3
Spectra 1000	C–C	16.0	15–17	0.3 ± 0.1
	C–G	15.4	15–16	0.5 ± 0.1
	G–G	15.4	15–16	0.4 ± 0.1
K-P drawn tape	C–C	23	18–32	0.3 ± 0.1
	C–G	18	16–21	0.5 ± 0.1
	G–G	19	16–22	0.4 ± 0.1
Spectra 1000 single fiber	C–C	26	20–37	0.4 ± 0.2
	C–G	20	17–23	0.6 ± 0.2
	G–G	21	18–25	0.5 ± 0.2

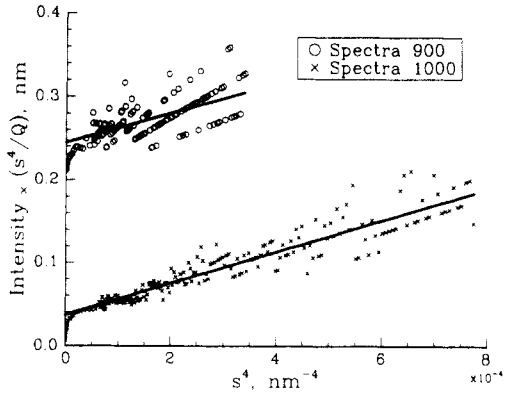

Figure 7. Porod plots of the intensity of the small-angle scattering along the equator, Is^4/Q vs s^4. The plots extend to s = 0.16 nm^{-1} for Spectra 1000 and 0.13 nm^{-1} for Spectra 900.

are close to those of Spectra 1000, but in Figure 6B the slope of the data is greater, giving a larger crystal width W and a larger distortion parameter, ϵ. The results for all the various fitting methods are listed in Table III.

The Porod plots for Spectra 900 and Spectra 1000 fiber bundles are shown in Figure 7. The points lie on oblique straight lines because of digitization. The data for Spectra 900 have been shifted vertically by 0.2 nm for clarity. The data for Spectra 1000 are a very satisfactory fit to the theoretical straight line over a wide range of s. The Spectra 900 fiber is not quite so satisfactory. At moderate values of s the data are very noisy and do not make a good straight line. A much better straight line can be obtained by considering a narrower range of s, but theoretically it is the data at the highest values of s that should give the best agreement with Porod's law. The extruded and drawn tape scattering was very much weaker, so there was no choice but to restrict the range of s. Plots of restricted range, up to 0.0001 for s^4, are shown in Figure 8 for the extruded fiber and for Spectra 900. Again the Spectra 900 plot is displaced vertically for clarity, this time by 0.1 nm. The values obtained from eq 10 are given in Table IV.

All the results using the Cauchy + Gaussian fits (C–G) of eq 5 and 8 are summarized in Table V. In this table the results for β are divided by $\pi^{1/2}$ to give an estimate of the rms value of α, the angle of misorientation of the structure about the fiber axis. As discussed in the data analysis section, this is the parameter commonly used to describe orientation, but the factor used to get it assumes a Gaussian distribution of orientations. In the SAXS case, it also assumes that the fibril interfaces are perpendicular to the fibril axis. Where two values for width have been obtained by Porod analysis, they are combined in Table V.

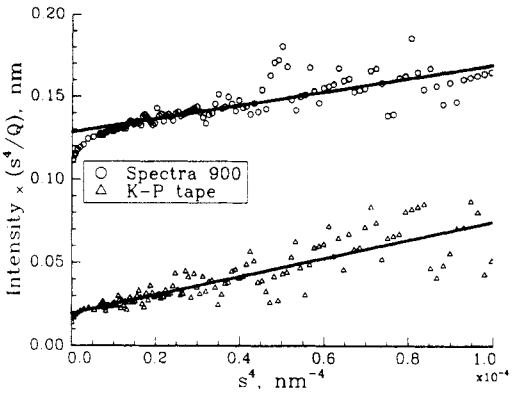

Figure 8. Porod plots of the intensity of the small-angle scattering along the equator, Is^4/Q vs s^4. These plots for Spectra 900 and for extruded and drawn tape are limited to s = 0.1 nm^{-1}.

Table IV
Results of Porod Analysis

range of s	spectra 900 width, nm	spectra 1000 width, nm	K-P tape width, nm
high, Figure 7	4.7 ± 0.3	5.2 ± 0.2	
low, Figure 8	6.7 ± 0.2	5.9 ± 0.1	19 ± 2

Table V
Summary of Numerical Results

sample	object measd	length, nm	width, nm	misorientation rms α, deg
Spectra 900 bundle	fibril	175 ± 25	5.7 ± 1.0	7.3 ± 0.5
	crystal	5–13	13 ± 1.5	2.1 ± 0.3
Spectra 1000 bundle	fibril	177 ± 10	5.5 ± 0.3	2.8 ± 0.2
	crystal	15–43	15.5 ± 0.6	1.4 ± 0.2
single fiber	crystal	22–1200		0.9 ± 0.1
K-P tape	fibril	195 ± 15	19 ± 2	0.3 ± 1.1
	crystal	18–60	18 ± 2	0.9 ± 0.1

Discussion

(a) Axial Lengths. It can be seen from Table V that the fibril length is in the range 150–200 nm for all samples. The different fibers are all quite similar in this. The precision of the results, for example 177 ± 10 nm (Spectra 1000), should not be misinterpreted as meaning that all the fibrils are of this length. The result is the volume-weighted average of a distribution of lengths, and this distribution is not known. The average is obtained on the basis that the line broadening due to fibril size is Cauchy in form. This form implies that the distribution is broad.

The crystal length is less accurately determined; for the extruded and drawn tape and for Spectra 1000 as measured here it is in the range 4–10 times less than the length of the fibril. Spectra 900 has a smaller crystal length, 3 times smaller than that of Spectra 1000 and thus 12–40 times less than the fibril length in Spectra 900. Measurement of the width of the (002) reflection is the method normally used to determine L, even though a series of (00l) reflections is necessary to distinguish crystal size from distortion effects. The (002) profile of a fiber of Spectra 1000 was previously determined during experiments on the effect of stress on the X-ray line shape.[24] The results were not analyzed in terms of crystal size at that time. At low applied stress, the integral breadth of (002) is 0.2° = 3.5 mrad. This by itself corresponds to an axial length $L = \lambda/(\mathrm{IB}\cos\theta)$ = 35 nm. Note that Murthy et al. show a (002) width of 0.4°,[25] and Smook and Pennings[26] derive a crystal length of 70 nm from the fwhm of (002). Despite this wide range of values for the crystal length, the SAXS length is longer than all of them.

The difference between the SAXS and the WAXS results for axial length is perfectly in accord with expec-

tation according to the standard model for a polymer fiber. In this model the microfibrils contain a number of crystals in series with less well organized and softer material. If the crystals and the amorphous domains have regular sizes, the repeat gives rise to a maximum on the small-angle scattering on the meridian. Applying Bragg's law to this maximum gives the "long period" repeat distance. Gibson et al.[27] found that the axial crystal length was greater than this long period for some stiff PE fibers. They based a fiber model on this fact, where the crystals extend through (bridge) the disordered regions, becoming more continuous. The high-modulus materials used here show no such maximum; indeed no meridional scattering is observed at all. The lack of scattering means that there is little density fluctuation in the axial direction on the scale we can observe. Scattering due to the 200-nm fibril length would be at 0.04°, too close to the main beam to be measured.

The presence of an equatorial SAXS streak similar to those in rigid-rod polymer fibers[24] indicates long fibrous objects, but the axial crystal size measured by the (002) line width is not very large. The results presented here show that there are long microfibrils containing smaller crystals in high-modulus fibers. How can this structure have a modulus close to the crystal modulus? This requires that the disordered zone that separates two crystals be very small, partially ordered, or both of these. The crystalline regions will appear as two distinct crystals in WAXS if the diffraction from them is not coherent; this requires atomic displacements only on the scale of angstroms or twists on the order of a degree. Such small changes need not make the regions mechanically discontinuous and would produce little small-angle scattering.

(b) Orientation. Consider first the crystal orientation in single fibers and tapes. For both the Spectra 1000 single fiber and the extruded and drawn tape, the integral breadth of the distribution of ($hk0$) plane normals, β, is 1.5° (Table I). Taking the orientation distributions to be Gaussian, the rms value of the molecular chain axis orientation about the fiber axis, α, is then 0.9 ± 0.1°. These are extremely well oriented materials, with an orientation function of 0.9996. A recent WAXS study of a bundle of Spectra 1000 fibers has given a variance for the axial misorientation of 0.69°.[23] This corresponds to an integral breadth β of 1.2 ± 0.1° for the assumed Gaussian distribution, in reasonably good agreement with the single-fiber result. The bundle used in ref 24 must have contained extremely parallel filaments.

Comparing the Spectra 1000 single fiber with the bundle of the same fibers, the crystal orientation declines from $\alpha = 0.9$ to 1.4°. As the distributions are taken to be Gaussian, the misalignment of fibers in the bundle is simply $(1.4^2 - 0.9^2)^{1/2} = 1.1°$. The SAXS fibril misorientation in the bundle can then be corrected to $(2.8^2 - 1.1^2) = 2.6°$ for the single fiber, but the effect of the correction is small. There are no data for single fibers of Spectra 900 but the effects of fiber alignment in a well-made bundle cannot be very important. This is because the misorientations that are found are comparatively large. For example, a 1° fiber misalignment, as in the Spectra 1000 bundle, would change the crystal and fibril misorientations from 2.0 and 7.3° to 1.7 and 7.2°.

Whether considering the results from Spectra bundle samples or the corrected values for single fibers, it is clear that the orientations of crystals and fibrils are different. In the standard view when the fibrils are approximated by cylinders or other prisms, this would be difficult to explain. If anything, the crystals would be expected to be misoriented with respect to each other in every fibril. This would require a greater misorientation for the crystals than for the fibrils. The simplest explanation for the observed greater misorientation in SAXS is that the method detects individual interfaces. If the microfibril has a nonuniform cross section of any kind, then the interfaces will be tilted further away from the fiber axis than the microfibril direction. Thus the orientation of the microfibril axes could be as good as that of the crystals, or better, but the small-angle scattering would show a worse orientation. In the case of Spectra 1000 the interfaces are tilted 1.4° more than the crystals, on average. Modeling the fibril as a pair of truncated cones, base to base, this tilt of the interface over a length of 177 nm would give a small increase in diameter at the center, of 4 nm. So for an average width of 6 nm, the fibril could change from 8-nm diameter at the center to 4 nm at the tips.

For Spectra 900 there is a discrepancy of the same type, but it is much greater. The crystal rms misorientation is 2.1° and the SAXS misorientation is 7.3°, so that the interfaces would have to be tilted 5.2° on average. For a microfibril in the shape of a pair of truncated cones, the diameter would increase by 16 nm at the equator. This model does not appear reasonable, since the width of the fibril (6 nm) is less than half of this. However, the width obtained from Porod's law is a different average of size and depends on the poorly known fibril volume fraction as discussed below. Alternatively, there may be smaller scale changes in the interface orientation, that is, a less regular microfibril shape.

Measurement of the rms misorientation angle α in SAXS is imprecise in the case of the extruded and drawn tape, so that the values of α for the crystals and for the microfibrils could be the same at 0.9°.

(c) Width. On a simple microfibril model of the polymer fibers one would expect the fibril diameter and the crystal widths to be the same. This is what we see for the extruded and drawn tape, when SAXS and WAXS both give a width of 18 nm. On *any* microfibril model of the polymer fibers one would expect that the fibril diameter should be greater than or equal to the crystal width, since the crystals lie in the fibrils. In the Spectra samples the fibril width is apparently less than the crystal size. There are at least two possible reasons for this, which do not require abandoning the basic model. One is that the fibril width derived from eq 9 is proportional to $1/(1 - \phi)$, where ϕ is the fibril volume fraction. This should be greater than the crystallinity, but it has no clear upper bound before 1. It was set to 0.9 in the calculations on the basis of structural information from Raman spectroscopy and as a reasonable estimate. We have only to set it to 0.95, as for the extruded and drawn tapes,[16] and the values for fibril width will double to 11 nm. This is a more normal value for fibril size in PE and allows a simple fibril shape to model the interface misorientation. However, this would mean that only a quarter of all the disordered material is in the interfibrillar regions, the rest of it being within the fibrils. This does not seem reasonable, particularly as the interpretation of axial crystal lengths above implies that the disorder in the fibrils is limited.

The other reason depends on the fibrils havig a wide distribution of sizes. The integral breadth of a WAXS reflection gives the volume-averaged size of the crystals. If there is no correlation between the length and the width of individual crystals, then the volume average width will be the same as the cross-section weighted average. This is the equivalent of weight average in molecular weight. If the crystals tend to have constant shape, the volume goes as width cubed, and the average will be the equivalent of z average in molecular weight. The Porod plot considers the interfaces between fibril and interfibrillar disordered material individually, without any regard to correlations. The derived mean diameter $\bar{D}$ is thus the number-average

diameter. The simplest structure that gives a broad distribution of fibril diameters is one where the interfaces are randomly placed in the fiber. The fibril sizes then have a most probable distribution, there the ratio of weight average to number average is 2 and the ratio of z average to number average is 2.6. Note that as the experimental results for the extruded and drawn tape agree, there cannot be a wide range of fibril sizes in this sample if the correct value has been chosen for ϕ.

(d) General. If the small-angle scattering comes from all three phases, crystal, disordered material, and voids, there might be a bimodal distribution of orientation or size of the scattering object. There was no evidence in any of the orientation distributions or in any line shape for such a bimodal distribution, so this study gives no basis for an attempt to go beyond a two-phase model for these materials.

When the small-angle scattering objects are taken to be voids, the volume fraction ϕ will be low, as the fibers are strong and dense. Then $1/(1 - \phi) \rightarrow 1$ and the lateral width derived from the Porod analysis becomes 0.5–0.6 nm for Spectra fibers and 2 nm for the extruded and drawn tape. As the calculated length and orientation are unaffected by changes in ϕ, the result would be narrow voids, down to the width of a molecule, with aspect ratios of 300:1. Although they are so elongated, these voids are not as well oriented as the crystals, which have a low aspect ratio between 1:1 and 3:1. Even though the crystals are known to be of limited size in the fiber direction, there is no detectable scatter from them at small angles. These implications all count against interpretation of the scattering as being due to voids.

Taking the small-angle scattering objects to be fibrils, the interfibrillar material will form a sheet only 0.3–0.4 nm thick. In this case the narrow structure is not empty but contains disordered polymer chains, so it cannot collapse. Not all of the structural parameters of the fibrils are in agreement with the expectations of a simple microfibril model. Slight modifications to that model, allowing nonuniform crosssections in fibrils and increasing the volume fraction of fibrils, can bring them into agreement, as discussed above. These problems should not be taken as strong evidence that the small-angle scattering is due to voids, as there is no equivalent structural model predicting the void shape and size. Interpretation of the SAXS in terms of fibrils does not mean that there are no voids, as a small fraction would not be detected if they were large (100 nm) or unoriented.

Conclusions

The numerical results for the PE samples studied here have already been summarized in Table V. As discussed above, the precise results given there depend on simple assumptions about line profiles. Without these assumptions, we can still say that the objects producing the SAXS streak are 150–250 nm long in all the specimens, with an average misorientation varying from 0 to 13°. The information on crystal size and orientation agrees with previous results and is most useful for comparison with the SAXS data. The comparison shows that the crystals are much shorter and equally or better oriented than the small-angle scattering objects.

The best interpretation of the small-angle scattering seems to be that it is produced by microfibril boundaries in these samples. The length derived is that of straight segments of fibril boundary, a lower limit for fibril length. Electron microscopy shows fibrils microns long,[28] but they need not have straight boundaries. Fibril width is found to be 5–20 nm, but these numbers depend on model parameters, not well-known.

Analysis of the SAXS equatorial streak giving length, orientation distribution, and mean separation of fibril boundaries should be applicable to any fiber with few voids, though interpretation will be numerically complex if the orientation is not very good. The SAXS data used here were taken from a single film, and the limited dynamic range limited the accuracy of the results. Clearly, data at the smallest scattering angles are best for extrapolation to (000) for fibril size, while data at larger angles give better information on orientation. However, the intensity is falling very rapidly with scattering angle. Multiple films with improved accuracy of registration or electronic detection with a wider dynamic range could provide information about larger objects, limited by the X-ray optics, in this case to a size of about 600 nm.

Acknowledgment. We are grateful for the support of this work by the NSF, DMR, through the Cornell Materials Science Center and for the access to the Cornell High Energy Synchrotron Source (CHESS). Thanks are due Dr. D. Bilderback and the rest of the CHESS staff for their continuing interest and assistance.

References and Notes

(1) Statton, W. O. In *Newer Methods of Polymer Characterization*; Re, B., Ed.; Interscience: New York, 1964.
(2) Glatter, O.; Kratky, O. *Small Angle X-ray Scattering*; Academic Press: London, 1982.
(3) Vonk, C. G. In *X-ray Scattering of Synthetic Polymers*; Balta-Calleja, F. J., Vonk, C. G., Eds.; Elsevier: Amsterdam, 1989.
(4) Vonk, C. G. *Colloid Polym. Sci.* **1979**, *257*, 1021.
(5) Adams, W. W.; Briber, R. M.; Sherman, E. S.; Porter, R. S.; Thomas, E. L. *Polymer* **1985**, *26*, 17.
(6) Kifle, Z.; Harrison, I. R.; Herman, R. M. *J. Polym. Sci., B: Polym. Phys.* **1986**, *24*, 633.
(7) Cakmak, M.; Spruiell, J.; White, J. L.; Lin, J. S. *Polym. Eng. Sci.* **1987**, *27*, 893.
(8) Grubb, D. T. In *Developments in Electron Microscopy and Analysis, 1977*; Misell, D. L., Ed.; Conf. Ser. Number 36, Institute of Physics: Bristol and London, 1977; p 399.
(9) Grubb, D. T.; Prasad, K.; Adams, W. W. *Polymer* **1990**, *32*, 1167.
(10) Hoogsteen, W.; Pennings, A. J.; ten Brinke, G. *Colloid Polym. Sci.* **1990**, *268*, 245.
(11) Statton, W. O. *J. Polym. Sci.* **1956**, *22*, 385.
(12) Ruland, W. *J. Polym. Sci., Polym. Symp.* **1969**, *28*, 143.
(13) Perret, R.; Ruland, W. *J. Appl. Crystallogr.* **1969**, *2*, 209.
(14) Perret, R.; Ruland, W. *J. Appl. Crystallogr.* **1970**, *3*, 525.
(15) Dobb, M. G.; Johnson, D. J.; Majeed, A.; Saville, B. P. *Polymer* **1979**, *20*, 1284.
(16) Kanamoto, T.; Tsuruta, A.; Tanaka, K.; Takeda, M.; Porter, R. S. *Macromolecules* **1988**, *21*, 470.
(17) Hoogsteen, W.; ten Brinke, G.; Pennings, A. J. *J. Mater. Sci.* **1990**, *25*, 1551.
(18) Kaji, A.; Ohta, Y.; Yasuda, H.; Murano, M. *Polym. J.* **1990**, *22*, 455.
(19) Perret, R.; Ruland, W. *J. Appl. Crystallogr.* **1968**, *1*, 308.
(20) Klug, H. P.; Alexander, L. E. *X-ray Diffraction Procedures*; Wiley: New York, 1974.
(21) Crist, B. *J. Appl. Crystallogr.* **1979**, *12*, 27.
(22) Porod, G. *Kolloid Z. Z. Polym.* **1952**, *125*, 108.
(23) Busing, R. *Macromolecules* **1990**, *23*, 4608.
(24) Prasad, K.; Grubb, D. T. *J. Polym. Sci., B: Polym. Phys.* **1990**, *28*, 2199.
(25) Murthy, N. S.; Correale, S. T.; Kavesh, S. *Polym. Commun.* **1990**, *31*, 50.
(26) Smook, J.; Pennings, A. J. *Colloid Polym. Sci.* **1984**, *262*, 712.
(27) Gibson, A. G.; Davies, G. R.; Ward, I. M. *Polymer* **1978**, *19*, 683.
(28) Schaper, A.; Zenke, D.; Schultz, E.; Hirte, R.; Taege, M. V. *Phys. Status Solidi A* **1989**, *116*, 179.

Registry No. PE (homopolymer), 9002-88-4.